Progress In Electromagnetics Research B, Vol. 93, 87–109, 2021

Dual Feed Multiband Microstrip Patch Antenna Design with Circular Polarized Wave for 5G Cellular Communication

Rajiv Pathak[1], Biswa Binayak Mangaraj[2, *], Arun Kumar[1], and Sushil Kumar[3]

Abstract—This paper proposes an orthogonal dual-feed microstrip patch antenna (MPA) that achieves multi-band resonance along with circular polarization at its primary band of 5G cellular communication. The proposed antenna is simpler than other designs to fulfill extreme data rates and minimum infrastructure requirements. This MPA is designed by taking most care for maintaining the isolation between ports with feasibility for physical fabrication. The HFSS based optimally designed proposed MPA resonates simultaneously at 3.48 GHz (3.3 GHz–3.7 GHz) band, 6.24 GHz (5.925 GHz–6.425 GHz) band, and 7.5 GHz (7.11 GHz–7.9 GHz) bands. The modes achieved for these three bands are TM_{01}, TM_{11}, and TM_{12} for 3.48 GHz, 6.24 GHz, and 7.5 GHz, respectively. The bandwidths achieved for the bands mentioned above are 160 MHz (4.57%), 330 MHz (5.27%), and 340 MHz (4.53%), respectively. The corresponding gains achieved are 9.8 dB, 5.06 dB, and 7.58 dB. The proposed MPA structure prototype is fabricated, and its performances are measured. The measured S_{11} for fabricated MPA is close to the resonating frequency found using HFSS simulation. The proposed MPA structure is also modeled and simulated in a MATLAB simulation environment. Performance parameters of the proposed MPA obtained in MATLAB and HFSS are compared and matched reasonably. The proposed MPA structure and its arrays are used for 5G cellular sites as a real-time application in a MATLAB simulation environment. Different test scenarios are created in MATLAB. SINR is visualized for the entire cellular area, and signal strengths are also fetched at the receiver sites.

1. INTRODUCTION

The demand for data usage grows exponentially due to the pandemic situation like Covid-19. High-speed data is the only alternative to overcome our mollified working due to the pandemic. Suddenly, the need for everything online and work from home are the only options for organizations or individuals. More and more people or services are going online to be future-ready for such a situation and accommodate the growth in data rate. The technological development responsible for constant data growth is human-to-device (H2D) interaction along with the preexisting device-to-device (D2D) and human-to-human (H2H) in 4G. Nowadays, 4G provides a higher data rate than previous generations due to the packet-switched network with a higher spectral band of 1.7 GHz–2.1 GHz with a moderate bandwidth of nearly 400 MHz. This available bandwidth fulfilled the requirement of a high data rate in 4G and coined device-to-device (D2D) realization [1–4] along with H2H (voice) communication. Human to a device (H2D) interaction [5] is another recent trend that will lay down a strong foundation for Internet of Things (IoT)-based automation [6, 7]. However, the data rate is insufficient to facilitate this H2D interaction and peak demand due to any pandemic in the future. All these situations together needed an extremely high-speed data rate beyond 4G [8]. More high spectral bands addition to 4G requires restructuring the

Received 26 May 2021, Accepted 26 July 2021, Scheduled 9 August 2021
* Corresponding author: Biswa Binayak Mangaraj (bbmangaraj@yahoo.co.in).
[1] Bhilai Institute of Technology, Durg 491001, India. [2] Veer Surendra Sai University of Technology, Burla 768018, India. [3] Government Polytechnic, Barauni 851134, India.

cellular area. Therefore, it will be better to go for the next cellular generation with larger bandwidth available at a high-frequency spectrum.

5G at a high-frequency band and enhanced cellular capacity will have wider channel bandwidth essentially required for improved data rate. The bandwidth requirement of 600 MHz–800 MHz [9] is essential as per the current needs of 5G. International Telecommunication Union Radiocommunication (ITU-R) sector has recommended a few spectral bands from sub 6 GHz or above 6 GHz to fulfill this bandwidth requirement partially. These recommendations are the summary of the conclusion of World Radiocommunication Conference (WRC)-2019 [10]. According to the guidelines, frequency band 3.3 GHz–3.7 GHz in sub-6 GHz band is also suggested for 5G services. The consequences of a high spectral band for 5G have reduced coverage. It requires additional towers and backhauling infrastructure to connect these towers to cover the entire geographical area, leading to infrastructure and financial overhead. A few bands have already been used for mobile backhauling by several countries from the recommended bands for 5G by ITU [11–13]. These bands are in the frequency ranges of 5.925 GHz–6.425 GHz, 6.425 GHz–7.125 GHz, and 7.1 GHz–7.9 GHz, mainly in the above 6 GHz range [12, 13]. These bands follow the line of sight above 6 GHz [14, 15], an essential requirement for wireless mobile backhauling [14]. As mentioned above, several countries have started working on 5G services for the band suggested by ITU-R [10]. Opportunities are readily available for researchers, communication engineers, and hardware design engineers worldwide due to hardware changes. In addition to the above available option, another scope is to design a multi-band antenna that can simultaneously serve users' communication and backhauling services. This multi-band antenna is designed specifically for 5G cellular base transceiver stations (BTSs), for which fewer antennas are needed. 5G cellular with low costing towers (LCT) enabled with such a multi-band patch antenna (MPA) needs to reduce overall launching costs. The low-cost, small size, and light weight properties of the MPA [16] make it suitable to fulfill the requirement, as discussed above.

Ansys HFSS software tool and antenna toolbox of MATLAB provide an environment for electromagnetic modeling of the proposed MPA antenna. The modeling of the proposed single element MPA with dual-feed resonating at the desired bands [17, 18], as discussed above, is initiated in HFSS. The substrate used in this modeling is Roggers R03003 having a height of 0.25 mm. The dielectric constant of this Roggers RO3003 has excellent stability for various frequencies and temperatures. Dual-orthogonal feeds are delivered with equal amplitude and 90° out of phase to excite three different modes, and subsequently, circular polarization is achieved. The dual-feed is one of the most straightforward multi-band MPA design approaches [17, 18]. The feed location is an important parameter that decides the performance parameters such as isolation between two ports, polarization, and the antenna's physical fabrication. Initially, the coaxial feed location is calculated theoretically for the first feed (primary feed). At the same time, the second feed location is either selected on a random basis or as calculated theoretically. Subsequently, feed locations are optimized parametrically in HFSS to get the proper threshold value of isolation between ports, obtain polarized waves, and get the physical fabrication of MPA. The primary feed location is along the length, i.e., along the x-axis at 3 mm from the center. The other feed location is along the width, i.e., along the y-axis at 7.5 mm from the center. Optimized feed locations are updated to obtain the final MPA structure. After simulating the final MPA, the obtained best performance parameters are noted down and analyzed. Fabrication of the realized antenna and its results are measured and compared with HFSS simulation results. The same MPA structure is developed and applied in a realistic environment to create 5G cellular sites in MATLAB.

The proposed MPA resonates at three different frequencies, 3.48 GHz in 3.3 GHz–3.7 GHz, 6.24 GHz in 5.925 GHz–6.425 GHz band, and 7.5 GHz in 7.11 GHz–7.9 GHz. Out of these three bands, one of the bands in the sub 6 GHz range, i.e., 3.3 GHz–3.7 GHz, can be used from BTSs to user's communication in downlink directions. The other two resonance bands, 6.24 GHz in 5.925 GHz–6.425 GHz band and 7.5 GHz in 7.11 GHz–7.9 GHz bands above 6 GHz range, are proposed for backhauling connection between mobile BTSs either in uplink or downlink direction. The values of S_{11} achieved for these three bands are −27.77 dB, −28.8 dB, and −33.98 dB, respectively. The lower-upper frequencies for the resonance bands 3.48 GHz, 6.24 GHz, and 7.5 GHz are 3.40 GHz–3.56 GHz, 6.08 GHz–6.41 GHz, and 7.32 GHz–7.67 GHz, respectively. The bandwidths achieved for these bands, as mentioned above, are 160 MHz (4.57% of f_c), 330 MHz (5.27% of f_c), and 340 MHz (4.53% of f_c), respectively. Isolation achieved between ports at resonating frequencies, as mentioned earlier, is −17.89 dB, −10.58 dB, and

−17.21 dB, respectively. The noted gain and modes for different resonance frequencies at 3.48 GHz, 6.24 GHz, and 7.5 GHz are 9.95 dB, 5.06 dB, and 7.58 dB and TM_{01}, TM_{11}, and TM_{12}, respectively. Mode TM_{01} is the dominant mode at the lowest resonance frequency and is also responsible for right-hand circular polarization (RHCP) at the same band. The axial ratio value is less than 3 dB for the entire band at the resonance frequency 3.48 GHz. Therefore, the same band is circularly polarized and provides flexibility to the users' orientation. The circular polarization of this band is finalized according to the mode analysis and the obtained value of the axial ratio simultaneously. The other two backhauling bands are partially circularly polarized due to the simultaneous existence of circularly and linearly polarized features. However, the circularly polarized wave used for mobile backhauling at these resonance frequencies is not essential due to the static orientation of base station antennas. After analyzing the simulation result, the modeled MPA is fabricated, and results are measured in the laboratory using a network analyzer and an anechoic chamber. The values of S_{11} attained after measurement are −30.0185 dB, −26.5809 dB, and −28.1154 at corresponding frequencies 3.48 GHz, 6.16 GHz, and 7.44 GHz. Although the value of S_{11} shifts moderately due to fabrication error, a good match between measurement and simulated results validates the proposed MPA structure. Due to the unavailability of a real-time test simulation environment in HFSS, the proposed MPA is also developed and simulated in MATLAB. The S_{11} obtained in MATLAB are −14.95 dB, −22.82 dB, and −20.55 dB for a moderately deviated but reasonably matching pattern compared to HFSS at resonance frequencies 3.624 GHz, 6.06 GHz, and 7.368 GHz. This moderate shift of S_{11} values and resonating frequency between MATLAB and HFSS is due to a change in matrix type, matrix size, and techniques. Successively, MPA was developed and tested in a realistic environment for the 5G network in MATLAB. Simultaneously, signal-to-interference and noise ratio (SINR) maps and beamforming are visualized for different scenarios such as additional foliage path loss and heavy rain. For a better understanding of the proposed work, the flowchart is shown in Figure 1.

The organization of this article is explained in this section. The paper starts with threefold problem statements, i.e., Section 2. Next to this section available 5G spectrums and their applications, i.e., the first problem statement are discussed in Section 3. In Section 4, the second problem statement solution, i.e., minimized infrastructure overhead, is discussed. From Section 5 onwards the third problem statement begins. Section 5 elaborates the design and performance of the proposed multi-band antenna, followed by its result discussions in Section 6. Finally, in Section 7, a real-time environment is created using MATLAB, which shows the designed antenna's application. The conclusion is discussed in Section 8.

2. PROBLEM FORMULATION AND PROPOSED SOLUTIONS

- Identify the different spectral bands for 5G according to ITU-R suggestions. Co-relate these spectral bands for 5G applications based on their nature of propagation.
- Search for a unique solution to reduce infrastructure overhead for an increased number of BTSs in 5G.
- Design a multi-band antenna for the problem, as discussed earlier, which can be used simultaneously for communication between users and cellular BTSs.
- Create a real-time 5G application environment for the proposed antenna.

3. AVAILABLE SPECTRUM AND THEIR PROPOSED APPLICATIONS IN 5G

Communications of different varieties altogether like H2H, D2H, D2D essentially require too high a data rate. Improvement in the data rate to facilitate these services simultaneously indeed coins the 5G. To achieve a high data rate, spectral bands' requirement at high frequency becomes essential, which needs change in hardware and restructuring of the cellular area [11]. Shifting directly from the LTE band to the bands suggested for 5G has a massive gap in coverage, infrastructure, and hardware changes [11–13]. As per ITU-R suggestions, spectrums below 10 GHz are considered for different 5G cellular services to overcome this available gap [10]. Spectrums in the sub 6 GHz range are mostly occupied except 3.3 GHz–3.7 GHz, while a considerable range of frequency spectrums is available above 6 GHz [9, 10].

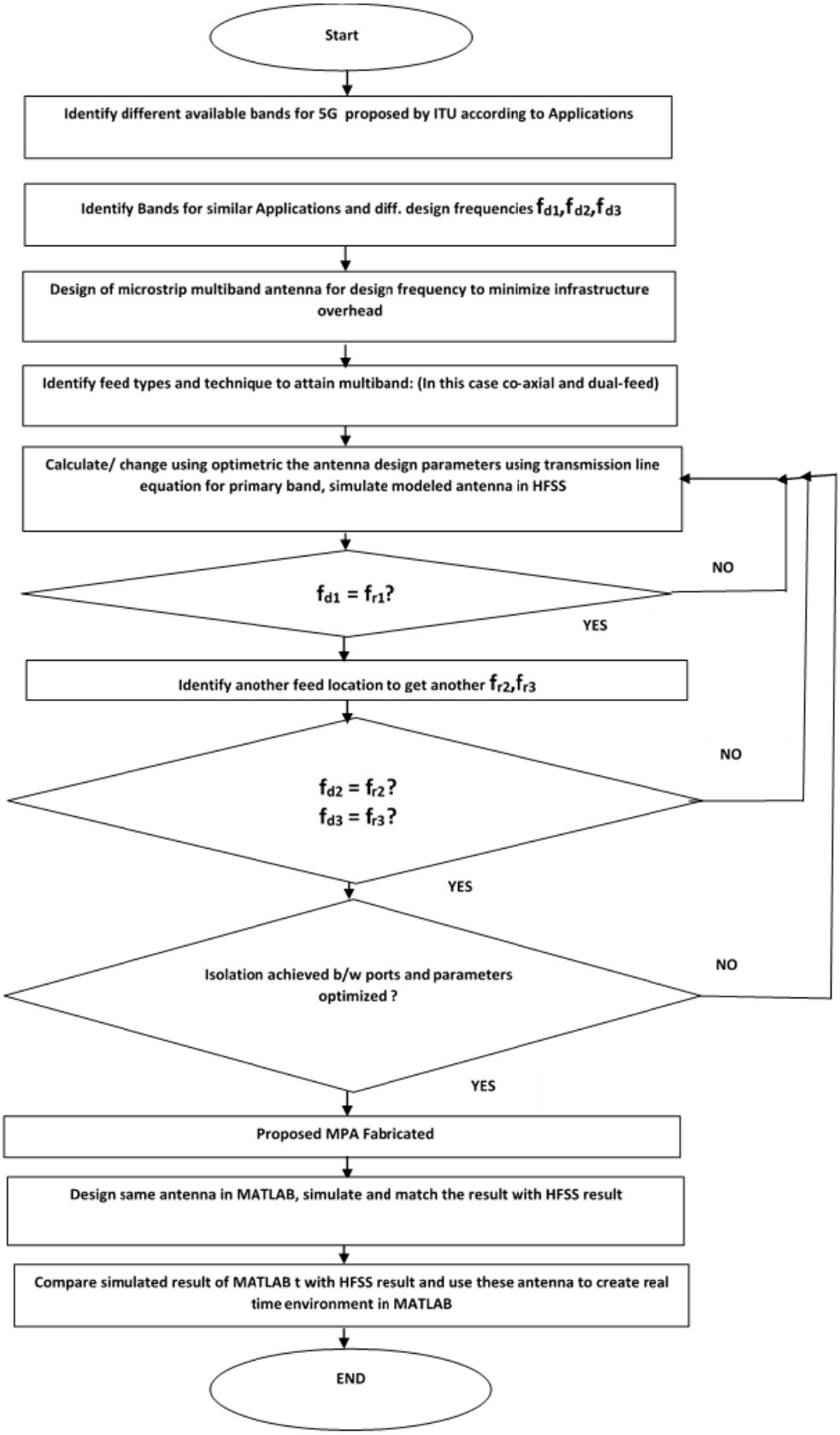

Figure 1. Flow-chart of the proposed steps of the proposed research work.

These available bands below 10 GHz are classified broadly into mobile user services [10] and fixed-mobile services [12]. Mobile user bands are dedicated to mobile users only, while fixed-mobile bands can be used either for fixed users or reserved for fixed transport services in mobile communication. Spectrum band 3.3 GHz–3.7 GHz is suitable for mobile users' communication where the line of sight is not needed. Line of sight (LOS) is essential for spectral bands 5.925 GHz–6.425 GHz, 6.425 GHz–7.125 GHz, and 7.11 GHz–7.9 GHz, i.e., above 6-GHz dedicated for transport services, i.e., mobile backhaul [12]. However, it is easy to maintain LOS due to the fixed location of BTSs. Applications and their propagation characteristics for the bands discussed above are listed in Table 1. The bands identified for mobile backhaul are used as a transport link for the interconnection of several BTSs.

Table 1. Different bands with their application and their propagation characteristics.

SI.No.	Band (GHz)	Typical application	Propagation Characteristic
1.	3.3 GHz–3.7 GHz	Mobile	NLOS
2.	5.925 GHz–6.425 GHz	Transport, mobile backhaul	LOS
3.	6.425 GHz–7.125 GHz	Transport, mobile backhaul	LOS
4.	7.11 GHz–7.9 GHz	Transport, mobile backhaul	LOS

Connecting each BTS to its neighboring BTS, a macro-base station, and extending this connection to remote BTS using mobile backhauling will create a cellular network. Cellular networks extend the services to remote location users and provide them seamless mobility for proper traffic load distribution. Uninterrupted service to mobile users, unassigned resource sharing between cellular regions, and communication services to distant places in cellular communication are only possible due to backhauling. The early age of the cellular system was supported by wired backhauling, while in mid-period wired and mobile backhauling were used, i.e., the backhaul's hybrid system. Several additional cellular BTSs are essential due to reduced coverage at high frequency in 5G [11, 13]. Wired backhauling to connect twenty times increased cellular towers, which requires extensive infrastructure, is quite expensive in 5G [13]. Mobile backhauling has the benefits of minimal infrastructure support, with less planning over wired backhauling demands broad assistance with colossal plan. Therefore, mobile backhauling for 5G cellular requires a reduced budget due to less planning and minimum required infrastructure. Simultaneously, it will compensate the overall launching cost for 5G cellular due to the financial overhead of increased cellular towers. Mobile backhaul must be used as a transport backbone network for voice and data traffic throughout the 5G cellular network to overcome the infrastructure issue [13, 14]. One essential mobile backhauling requirement is its required wideband spectrum with minimum propagation delay to transport massive amounts of data. Several spectral bands are presented in Table 1 for mobile backhauling along with propagation characteristics. Minimum propagation delay can be achieved due to wide spectral bands at high frequency range. These wide spectral mobile backhauling bands suggested for 5G communication create a 5G cellular network.

4. MINIMIZED INFRASTRUCTURE OVERHEAD WITH PROPOSED MULTIBAND MPA

An increased number of BTSs are needed in 5G cellular as per the enhanced cellular capacity requirement. These increased BTSs have a vast infrastructure requirement, such as additional towers, increased antennas on these towers, and backhauling solutions [11, 13]. These BTSs enabled with mobile backhauling, as discussed earlier, needed low expense in comparison to wired backhauling [14]. Mobile backhauling requires directional antennas with signal processing modules [14]. Several different antennas are necessary for communication and backhauling BTSs, which occupy a large area [14]. Single-band multiple antennas for communication and backhauling are replaced with a multi-band antenna resonating simultaneously at communication and backhauling bands, as our proposed MPA. Fewer proposed multi-band MPAs are needed than so many single-band antennas for user's communication and backhauling individually. Smaller number of these multi-band antennas require less space than

many single band antennas for the same application. Hence, these low costing BTSs enabled with our proposed MPA can minimize the infrastructure and financial overhead.

5. DESIGN OF CONVENTIONAL MPA AND PROPOSED DUAL-FEED MULTIBAND MPA

5.1. Conventional MPA

Microstrip Patch Antenna (MPA) is most popular due to its low cost, easy fabrication, light weight, mass production, integration with microwave circuits, and formal structure [16–18]. Low cost, easy manufacturing, and lightweight MPA [17] are preferable to fulfill the requirements mentioned above for LCT. Parameters like a dielectric constant (ε_r), the height of the substrate (H), operating frequency (f_0) are essential to calculating input design parameters such as patch length (L) and patch width (W). The substrate material has basic input parameters such as dielectric constant (ε_r) and height (H). Here Rogers RO3003 substrate material is considered to design a better quality multi-band antenna due to its dielectric constant stability over varying frequency. The dielectric constant (ε_r) of the Rogers RO3003 substrate is 3, and the loss tangent ($\tan\delta$) is 0.0013. The height of the substrate (H) is 0.25 mm. Input design parameters of the proposed MPA are calculated using transmission line Equations (1)–(7) [16, 17]. Feed location is also an important parameter that decides the performance of the antenna and is calculated using Equations (8)–(9) [17]. The top view of the conventional MPA is shown in Figure 2(a) with its dimensions. In Figure 2(b), a cross-sectional view of the MPA is demonstrated.

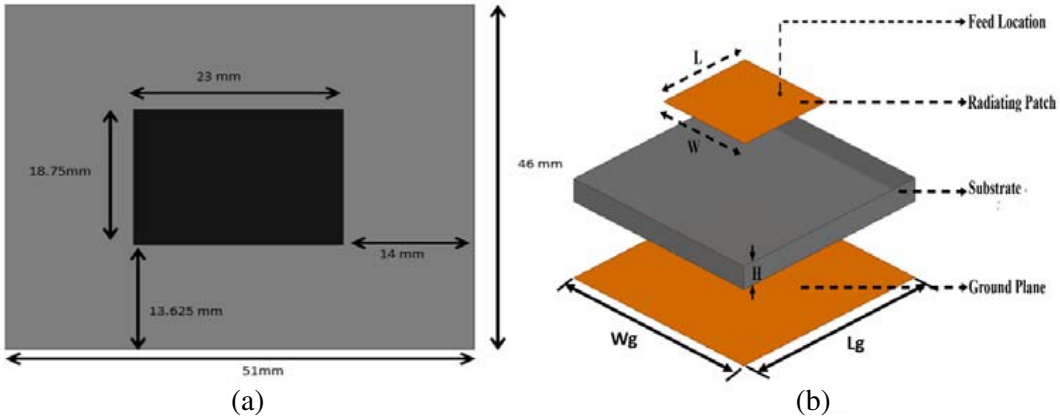

Figure 2. (a) Dimension of conventional MPA, (b) cross-sectional view of conventional MPA.

The length L_g and width W_g of the ground are given by,

$$Lg = L + 6H \tag{1}$$

$$Wg = W + 6H \tag{2}$$

The relation to calculate the width of the patch (W) is,

$$W = \frac{c}{2f_o\sqrt{\frac{(\varepsilon_r+1)}{2}}} \tag{3}$$

An approximate relation for effective dielectric constant ε_{reff} is,

$$\varepsilon_{reff} = \frac{\varepsilon_r+1}{2} + \frac{\varepsilon_r-1}{2}\left(1+12\frac{h}{W}\right)^{-\frac{1}{2}} \tag{4}$$

The effective length depends on the fringing effect and is given by the function of ε_{reff} and width to height ratio (W/h). A relation for normalized extension of the range is provided by,

$$\Delta L = 0.412h\frac{(\varepsilon_{reff}+0.3)\left(\frac{W}{h}+0.264\right)}{(\varepsilon_{reff}-0.258)\left(\frac{W}{h}-0.8\right)} \tag{5}$$

The following equations are used to calculate the effective, and the actual lengths of the patch are,

$$L_{eff} = \frac{c}{2f_o\sqrt{\varepsilon_{reff}}} \tag{6}$$

$$L = L_{eff} - 2\Delta L \tag{7}$$

Feed location of the co-axial feed can be approximated by the following formulae,

$$fl = L/4 \text{ (for Narrowband)} \tag{8}$$

$$fl = L/6 \text{ (for Wideband)} \tag{9}$$

Physical dimensions such as width, actual length, and electrical length of the MPA are calculated using Equations (1)–(7) [16], whereas feeding locations were initially calculated using Equations (8)–(9) [17], and their values are mentioned in Table 2. These computed values, as per theory, are initially used to design a single feed antenna and later modified to dual feeds, as discussed in the next section.

Table 2. Design parameters of dual-band MPA.

Parameter	Input Parameters (mm)						
	Length of Patch L	**Width of Patch W**	**Length of Ground Lg**	**Width of Ground Wg**	**Feed location of first feed (fl1)**	**Feed location of second feed (fl2)**	**Substrate height**
Theoretical	19.17	26.08	47.97	54.88	3.195	3.833	0.24
Optimized	18.75	23	47.55	51.88	3	7.5	0.24

5.2. Dual-Feed MPA Design

Dual-feeds are designed orthogonally in this proposed rectangular MPA, as shown in Figure 3, to excite multi-mode results in multi-band resonance operation. The first feed placed along the x-axis

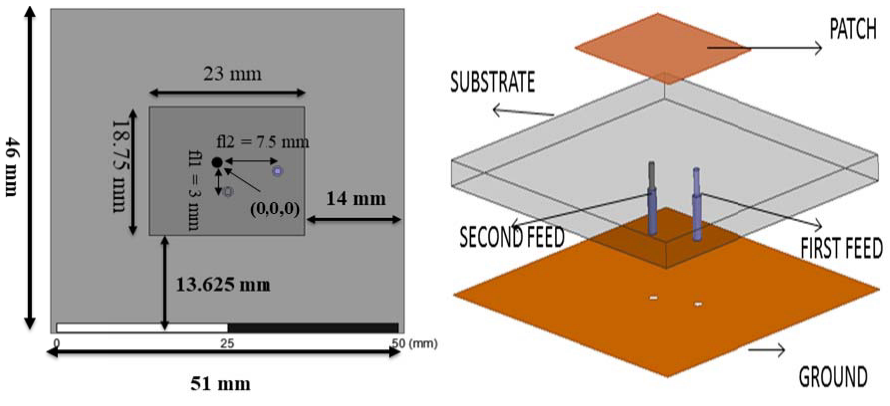

(a) (b)

Figure 3. (a) Front-view of dual-feed MPA, (b) cross-sectional view of dual-feed MPA.

and the second feed along the y-axis. These feed locations are calculated using either Equation (8) or Equation (9), depending upon narrowband or wideband applications. The approximate calculation of the dual-feeds is shown below

For 1st feed location in the x-axis:

$$fl = L/4 = 4.792\,\text{mm} \text{ to } fl = L/6 = 3.195\,\text{mm}$$

For 2nd feed location in orthogonal direction (if calculated theoretically):

$$fl = L/4 = 5.75\,\text{mm} \text{ to } fl = L/6 = 3.833\,\text{mm}$$

Optimize the feed locations to achieve desired resonance frequencies and isolation between two feed locations. Feed location is significant from a fabrication point of view too. Proper feed location will allow the realization of the physical fabrication of the antenna. These feeds are excited such that each feed receives equal amplitude of the signal with 90° out of phase.

5.3. Dual-Feed MPA Modeling in HFSS

The first feed location responsible for the first resonance band is supposed to be between 3 mm and 5 mm as per given Equations (3) and (4) [17]. The other feed location is initially calculated similar to the first feed although being optimized later to get better isolation between ports, other desired bands, and circularly polarized waves. After optimizing the second feed, the distance between the two ports should be such that the possible physical fabrication of the antenna becomes feasible. After theoretical analysis and calculation of designed parameters, modeling this particular structure starts in HFSS. The antenna is modeled in HFSS based on the design parameters obtained from theoretical calculations. After the simulation of the above antenna structure, the resulting performance parameters have a slight mismatch with the desired performance parameters. Simultaneously, parametric variations on other design parameters are applied to get the desired performance parameters. This variation in design parameters is implemented either individually or in group till the desired performance parameters

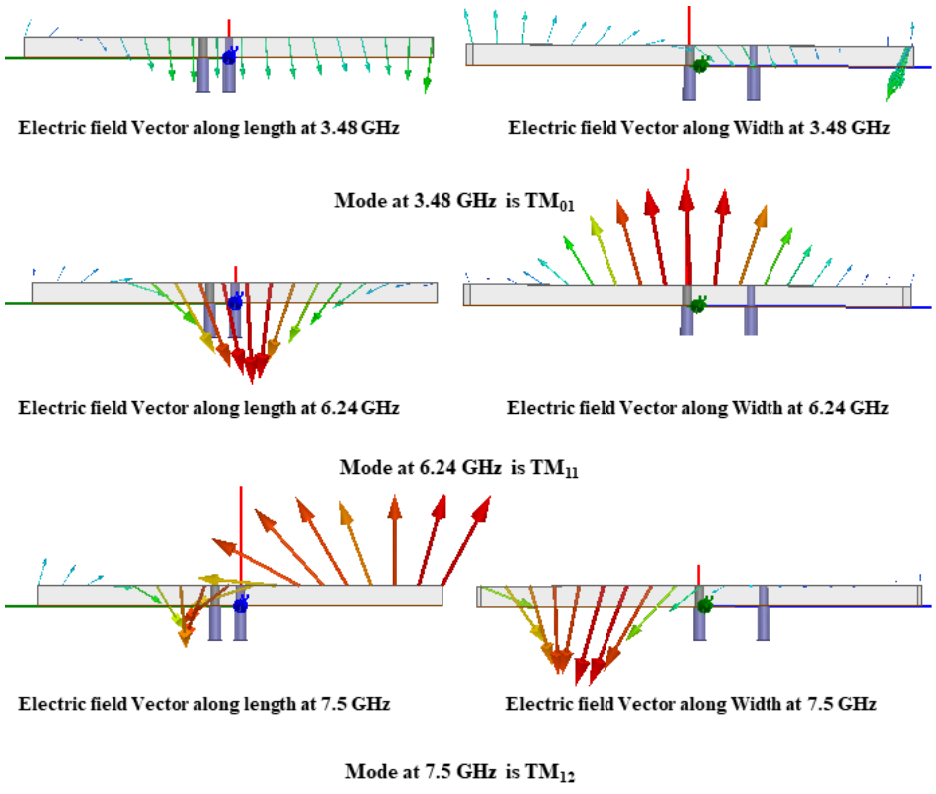

Figure 4. Modes at resonance frequencies 3.48 GHz, 6.24 GHz, and 7.5 GHz.

are achieved. The final structure of MPA is modeled according to the design parameters obtained after parametric optimization and simulated to achieve the expected performances. The final modeled MPA is analyzed for modes and their polarization at different resonance frequencies. The electric field variation along length and width is considered to determine its mode at the different resonance frequencies. In this case, the electric field is parallel to the direction of radiation. The magnetic field is perpendicular to the direction of propagation; hence the mode derived is TM, as shown in Figure 4, for all resonance frequencies of interest. The different wavelengths attained by these electric vectors along the length and width of the MPA at different resonance frequencies will decide the exact mode, as shown in Figure 4. For the proposed MPA structure, modes obtained are TM_{01}, TM_{11}, and TM_{12}, at resonance frequencies 3.48 GHz, 6.24 GHz, and 7.5 GHz, respectively, where TM_{01} is the dominant mode at the lowest resonance frequency of the antenna proposed. The simultaneous excitation of two orthogonal feeds with slightly larger patch width than patch length is responsible for introducing in-phase and out-of-phase signals [17]. These in-phase and out-of-phase signals excite even- and odd-order modes, respectively. The main reason behind exciting these three modes is to induce triple resonating bands in the proposed MPA. TM_{01} is responsible for the 3.48 GHz resonance band, whereas mode TM_{11} yields a 6.24 GHz band. Mode TM_{12} is accountable for the 7.5 GHz resonance band. In TM_{11} mode, half-wavelength field variations are along patch length and width. The circular polarization of the proposed antenna is achieved at 3.48 GHz due to the excitation of orthogonal feeds with equal amplitude and 90° phase shift. The modes TM_{01} and TM_{12} are the electric field variations along width and length, respectively; therefore, these modes are responsible for circular polarization in the proposed antennas.

Design parameters for best-valued performance parameters are noted and compared with theoretical parameters in Table 2. Later, the design parameters obtained theoretically are optimized to achieve desired performance parameters. Finally, after the simulation of the proposed MPA structure, performance parameters are presented in Table 3.

Table 3. Performance parameters at different bands.

Parameters	**Bands (GHz)**		
	3.3 GHz–3.7 GHz	**5.925 GHz–6.425 GHz**	**7.11 GHz–7.9 GHz**
Resonance frequency	**3.48 GHz**	**6.24 GHz**	**7.5 GHz**
S_{11}(-dB) in HFSS	−27.77	−28.8	−33.98
S_{12}(-dB) in HFSS	−17.89	−10.58	−17.21
Gain (dB)	9.95	5.06	7.58
10-dB return loss bandwidth	160 MHz, 4.57%, (3.40 GHz–3.56 GHz)	330 MHz, 5.27%, (6.08 GHz–6.41 GHz)	340 MHz, 4.43%, (7.32 GHz–7.66 GHz)
Radiation Efficiency	81%	77%	73.85%

5.4. Performance Parameters

Theoretical design parameters were utilized while the antenna was modeled in the HFSS environment. After simulation of this modeled antenna, some deviations were observed in its performances which were achieved using parametric optimization available in HFSS. However, conclusions finalized in this process were significant. The length of the antenna decides the resonance frequency of the antenna, and the relationship that exists is inverse. Resonance frequency also varies by varying dielectric constants. The resonance frequency initially increases due to an increase in substrate height (reduction in W/h ratio). However, the overall resonance frequency decreases due to a rise of ΔL [17]. Due to this reason the resonance frequency is inversely proportional to substrate height. However, the bandwidth is directly proportional to the height of the substrate. The width of the patch controls the impedance, bandwidth, and radiation pattern of the antenna. For better gain and bandwidth, the height of antennas is to be more while the value of the dielectric constant is required to be less. However, several constraints may exist for these input parameters depending on the applications of the antenna. According to desired

performances of the antenna, its design parameters are altered. Efficient and effective transmission and reception of signals by the antenna depend upon its performance parameters. Parameters such as the reflection coefficient, isolation parameters, input impedance, radiation pattern, gain, directivity, realized gain, and the axial ratio are analyzed for the proposed MPA. The reflection coefficient measures the reflected wave at the source-antenna interface due to impedance mismatch. It also decides the 10 dB bandwidth of the antenna. The isolation parameter is a vital parameter used in the multi-port antenna that measures interference between ports. Input impedance is a combination of resistive and capacitive loss measurements of the antenna. Radiation characteristics of the antenna make us visualize the radiated intensity in a particular direction. Gain, directivity, realized gain are measures of converting the input power to the radio wave, maximum gain in a specific direction, and actual realization of the gain, respectively. The gain and directivity of the antennas are utilized to calculate the radiation efficiency of the antenna [16]. The axial ratio measures the polarization of the generated wave. These performance parameters of the proposed MPA are discussed with plotted graphs in their following respective sections.

Reflection Coefficient (S_{11} in dB): This parameter deals with the reflected wave measurement due to the antenna's impedance mismatch. That is why it is commonly known as the reflection coefficient of the antenna. It is an essential parameter for antenna design and analysis. The reflection coefficient's value should be as minimum as possible close to its desired value of 15 dB. The reflection coefficient is useful for the calculation of the 10 dB return loss of the antenna. Figure 5(a) shows the reflection coefficient versus frequency graph for the modeled structure simulated in HFSS. From Figure 5(a), the gains at different resonance frequencies, 3.48 GHz, 6.24 GHz, and 7.5 GHz are −27.77 dB, −28.8 dB, −33.98 dB, respectively. The lower-upper frequencies for the first resonance band, 3.48 GHz, are 3.40 GHz–3.56 GHz. The lower-upper frequencies for the second resonance band of 6.24 GHz are 6.08 GHz–6.41 GHz, whereas the third resonance band of 7.5 GHz is 7.32 GHz–7.67 GHz.

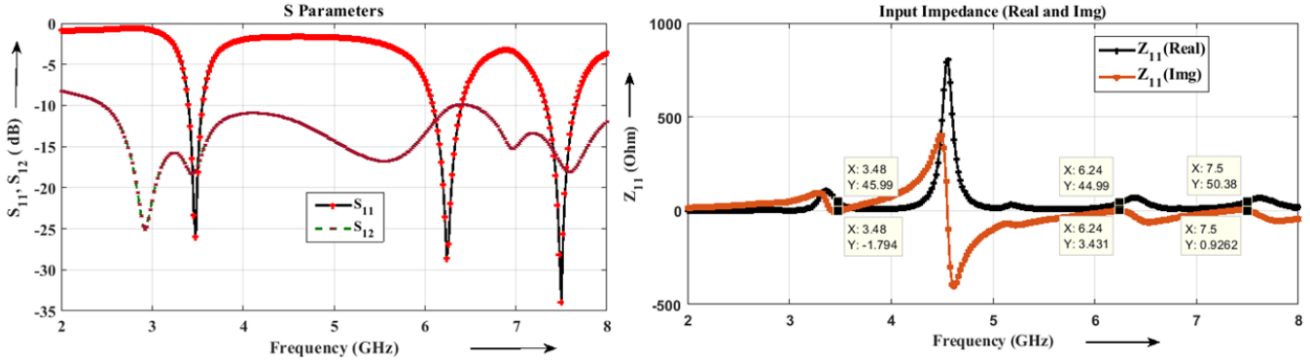

(a) (b)

Figure 5. Simulated (a) reflection-coefficients S_{11} and S_{12} vs. frequency, (b) impedance Z_{11} vs. frequency of dual-band MPA.

Isolation Parameter (S_{12} in dB): S_{12} is the measure of interference due to power transfer from ports 2 to 1. In other words, it is the measure of isolation between two ports. A better isolation will result in minimum impact of a port on the other port. In Figure 5(a), a graph is plotted in-between S_{11}, S_{12}, and frequency. The S_{12} isolation between two ports is −17.89 dB, −10.52 dB, and −17.21 dB at frequencies 3.48 GHz, 6.24 GHz, 7.5 GHz, respectively. The values achieved in our case are higher than the threshold value of $-10\,dB$ at desired frequencies.

Input Impedance (Z_{11} in Ω): Input impedance of the antenna is a measure of how efficiently power reception or transmission by the antenna is achieved at the desired frequency. Antenna impedance is a complex value having resistive and reactive parameters. The real part of this complex value is radiation resistance, while the imaginary part is known as the loss of the antenna. Hence for impedance matching, the matching network should have a complex conjugate of antenna impedance. Figure 5(b) shows the real and imaginary parts of impedance versus frequency. The input impedance values are

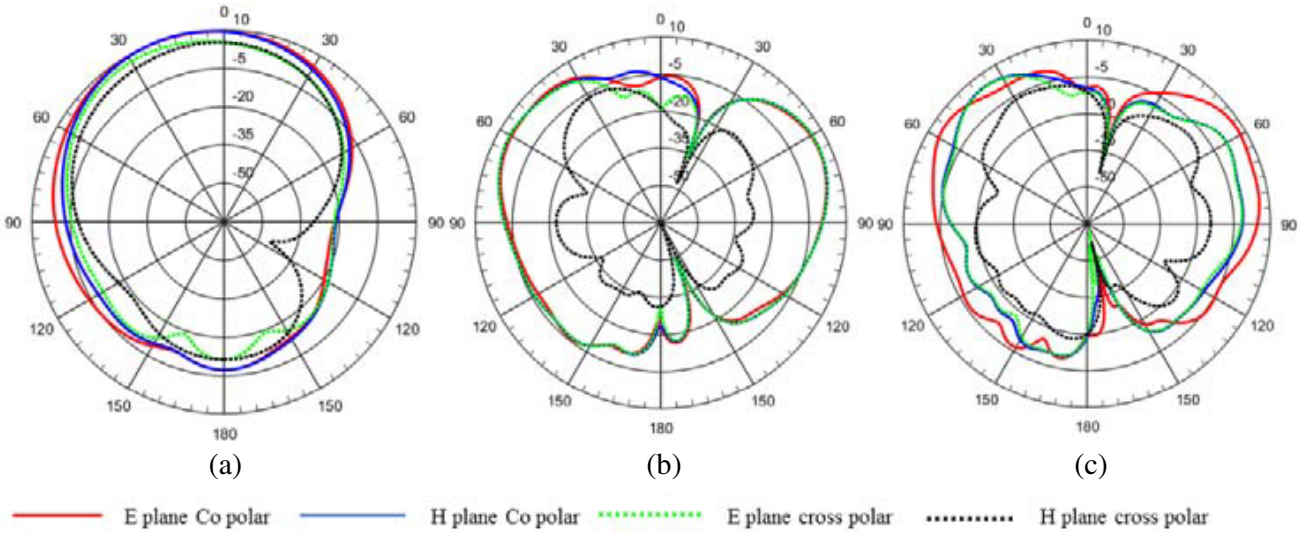

Figure 6. Radiation pattern co-polar cross-polar in E and H plane (a) at 3.48 GHz, (b) at 6.24 GHz, (c) at 7.5 GHz.

$45.99 + j1.794$ at 3.48 GHz, $44.99 + j3.431$ at 6.24 GHz, and $50.38 + j0.9262$ at frequency 7.5 GHz.

Radiation Pattern: The radiation pattern of the antenna is a radiated power intensity in a particular direction. It is the energy emitted at the transmitter antenna and energy received at the receptor antenna. Figures 6(a), 6(b), and 6(c) show the co-polar and cross-polar radiation patterns in the E-plane and H-plane at resonance frequencies 3.48 GHz, 6.24 GHz, and 7.5 GHz, respectively.

Gain, Directivity, and Realized Gain (in dB): Gain, directivity, and realized gain curves are plotted concerning the frequency shown in Figure 7(a). Gain of the antenna is a ratio of power transmitted in the direction of peak radiation to the power of that antenna as an isotropic source [25]. On the other hand, directivity measures the directional property of the antenna by calculating the radiation intensity in the direction of its maximum radiation [25]. Calculation of the antenna gain is possible while the efficiency of the antenna is multiplied with its directivity. Realized gain is a reduced gain when losses are considered due to a mismatch of input impedance [25]. Hence values of directivity, gain, and realized gain would be in decreasing order for an antenna. Respective gains are also noted down in Table 3 at three different resonance frequencies. The gains of the antenna at three different frequencies, 3.48 GHz, 6.24 GHz, and 7.5 GHz, are 9.95 dB, 5.06 dB, and 7.58 dB, respectively. Therefore, a good match in Figure 7(a) exists among Gain, Directivity, and Realized gain that validates these parameters.

Radiation Efficiency: Antenna efficiency is defined as a ratio of power delivered by the antenna to space to the input power supplied to the antenna. Before utilizing an antenna for practical applications, it is necessary to analyze the radiation efficiency of the antenna. The radiation of the proposed antenna at different resonance bands is presented in Table 3. A relationship between radiation efficiency and frequency is shown in Figure 7(a). From this relationship, it is concluded that the antenna resonates at the first resonance band, i.e., at 3.48 GHz with 81% radiation efficiency, while at the second and third resonance points of 6.24 GHz and 7.5 GHz, radiation efficiencies are 77% and 73.85%, respectively.

Axial Ratio: The ratio between the minor and major axes of the polarization ellipse is known as the axial ratio. If the curve has an equal major and a minor axis and is a case of the circle, then the antenna is said to be circularly polarized. An antenna is circularly polarized if the axial ratio's value is less than 3 dB. In Figure 7(b), a relationship plotted between the minimum axial ratio to the frequency bands mentioned above is analyzed for circular polarization based on the minimum axial ratio's obtained value. After field mode analysis, simultaneously achieving the value of axial ratio less than 3 dB and clockwise rotated field line distributions at different phase angles as shown in Figure 8, for band 3.3 GHz–3.7 GHz, satisfies the right-hand circular polarization (RHCP). The other two bands, 5.925 GHz–6.425 GHz and 7.11 GHz–7.9 GHz, are moderately polarized as their axial ratio values are partly less than 3 dB.

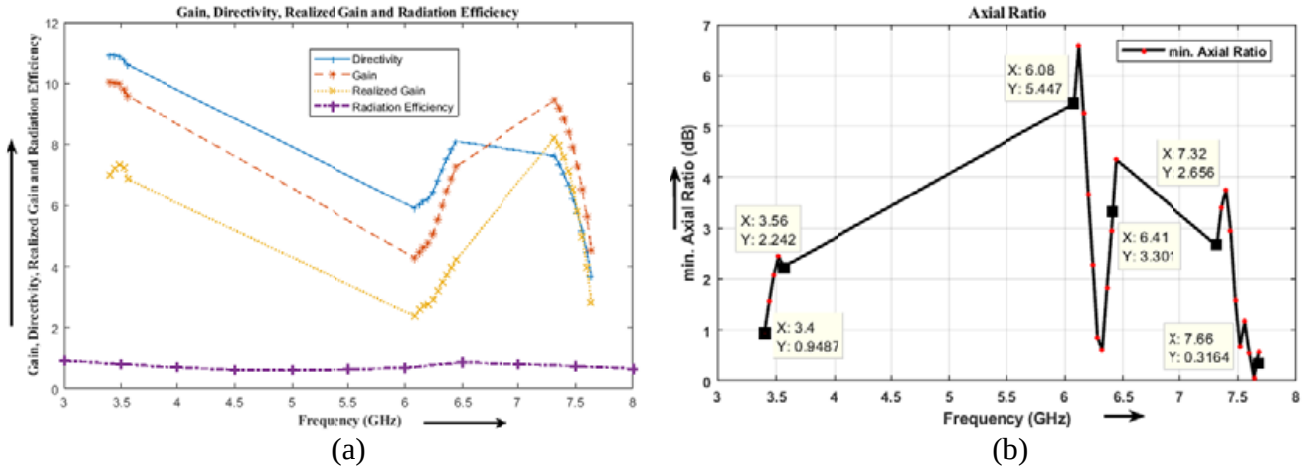

Figure 7. (a) Gain, directivity, and realized gain radiation efficiency vs. frequency, (b) axial ratio vs. frequency.

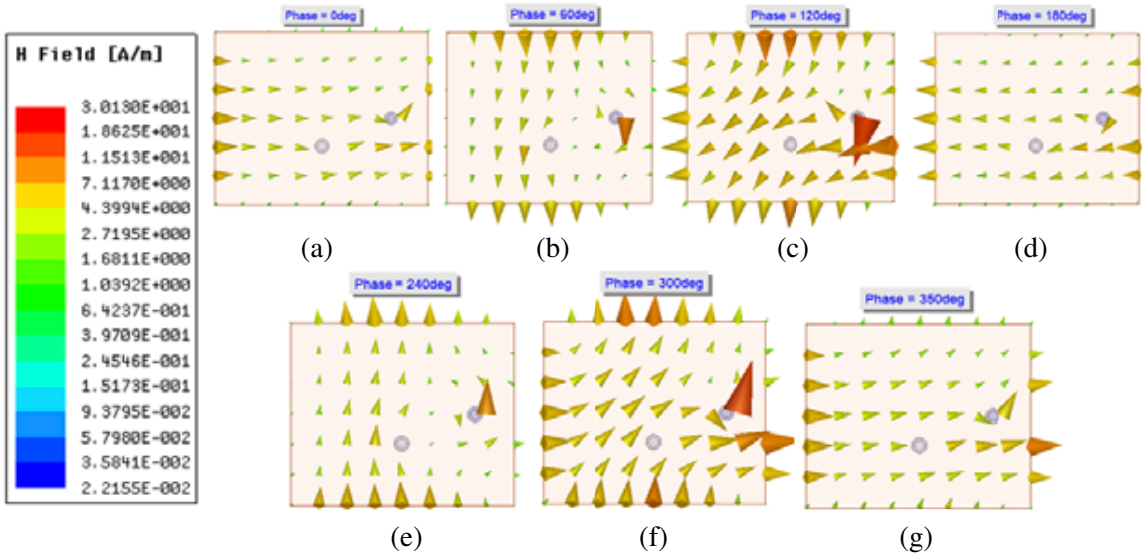

Figure 8. Field lines showing RHCP at different phases for the proposed MPA, (a) 0°, (b) 60°, (c) 120°, (d) 180°, (e) 240°, (f) 300°, and (g) 350°.

6. RESULT AND DISCUSSION

The optimized design parameters are considered in the fabrication of physical prototype of the proposed MPA structure. Figure 9 shows the fabricated antenna prototype with its design parameters, especially patch length and width. The antenna structure's front and back views are displayed with a scale to verify its physical dimension, with the simulated one presented in Table 2. The antenna's size is measured using a scale shown in Figure 9, compared with the simulation dimension indicated in Table 2. The Agilent N5247A network vector analyzer is used to measure the antenna's reflection coefficient, as shown in Figure 10(a). The antenna was tested in an anechoic chamber, as shown in Figure 11, and its performances were measured. An anechoic room is a closed environment where the antenna under test (AUT), placed as a receiver at a far-field location from the source antenna. Firstly, the horn antenna as a source antenna is positioned at the transmitter end and AUT as a receiver antenna is placed at a far-field distance from the source antenna. A fully automated environment inside an anechoic room is controlled by PCs. A transmitter antenna generates the correct frequency range, whereas a receiver

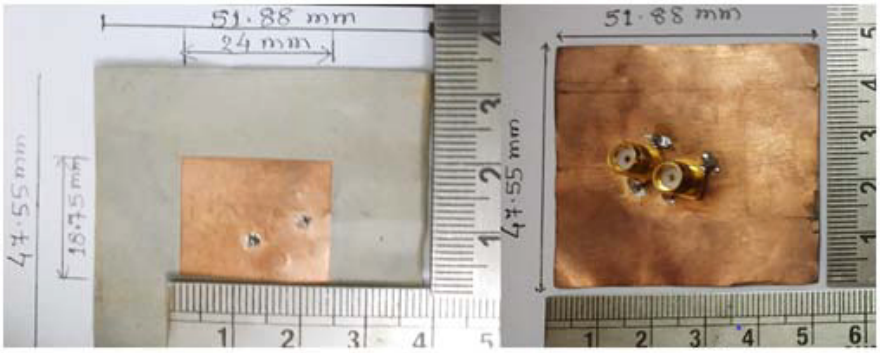

(a) (b)

Figure 9. Fabricated antenna prototype (a) front view, (b) back view.

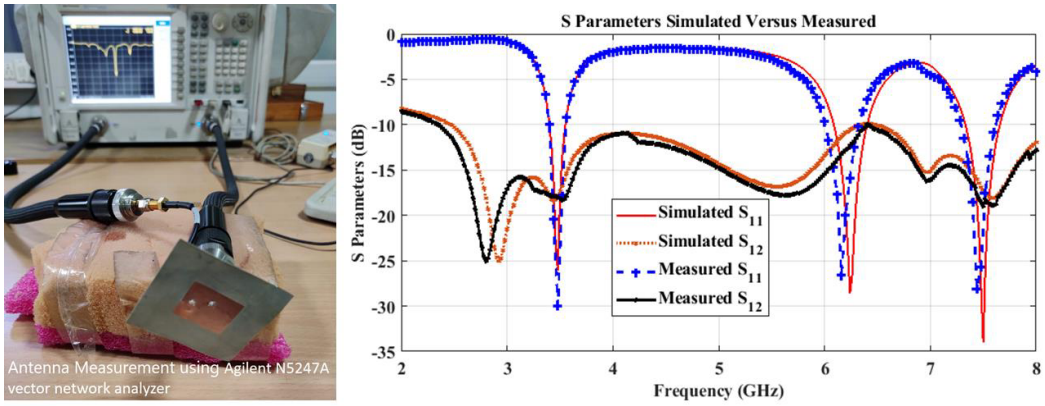

(a) (b)

Figure 10. (a) Antenna reflection co-efficient S_{11} measured in Agilent N5247A network vector analyzer. (b) Simulated and measured reflection coefficients, S_{11} vs. frequency.

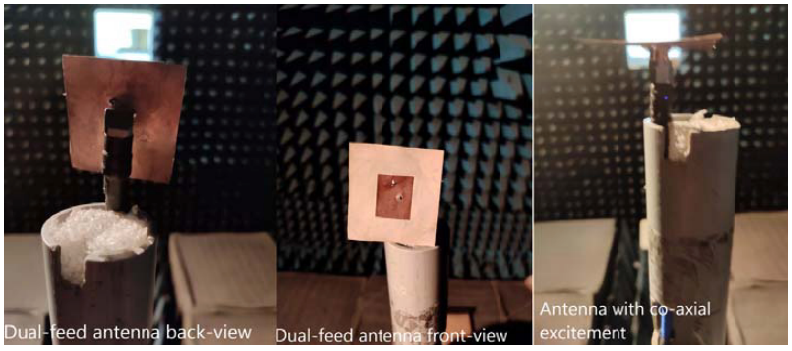

Figure 11. Antenna under test (AUT) in an anechoic chamber.

system measures AUT's signal. The positioning system is in the chamber, which can hold and rotate AUT to 360 degrees.

It is found that the measured and simulated values are closed to each other. Therefore, the measured values of resonance frequency and S_{11} are compared with the simulated ones presented in Table 4. The measured S_{11} obtained are -30.0185 dB, -26.5809 dB, and -28.1154 dB for corresponding frequencies

Table 4. Simulated and measured resonance frequency and reflection coefficient (S_{11} in dB) for different bands.

Band (GHz)	Simulated		Measured	
	Resonance frequency (GHz)	S_{11} (dB)	Resonance frequency (GHz)	S_{11} (dB)
3.3 GHz–3.7 GHz	3.48	−27.77	3.48	−30.0185
5.925 GHz–6.425 GHz	6.24	−28.8	6.16	−26.5809
7.11 GHz–7.9 GHz	7.5	−33.98	7.44	−28.1154

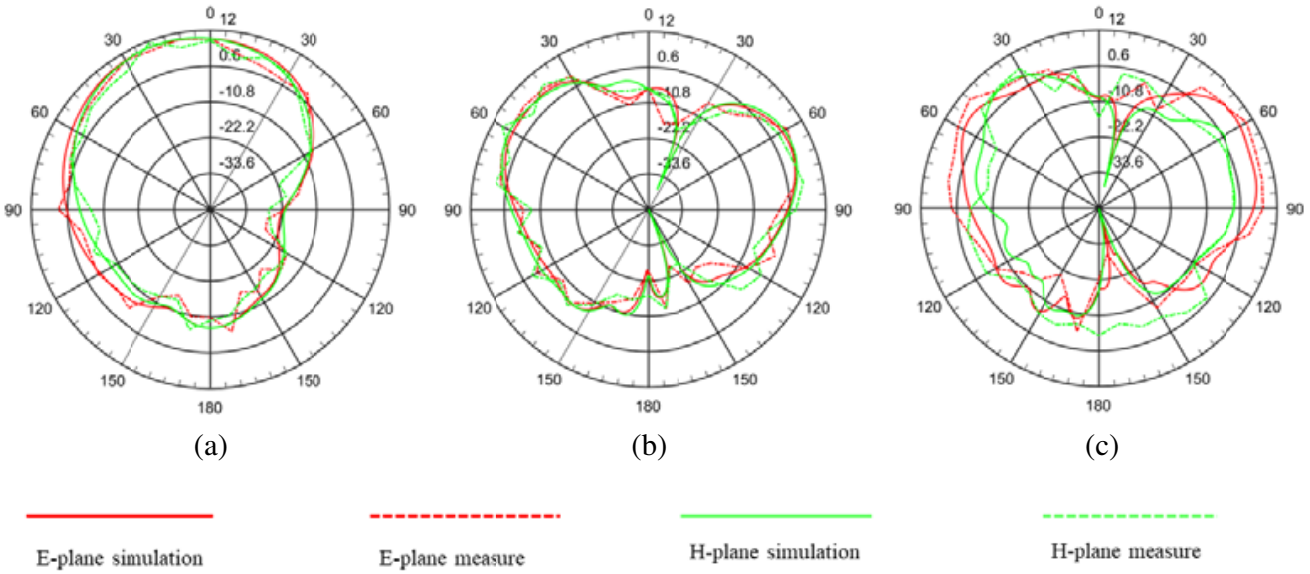

Figure 12. Co-polar radiation pattern for both E-plane and H-plane: (a) at 3.48 GHz, (b) at 6.24 GHz, and (c) at 7.5 GHz.

of 3.48 GHz, 6.16 GHz, and 7.44 GHz. The simulated S_{11} values of −27.77 dB, −28.8 dB, and −33.98 dB are at their corresponding frequencies of 3.48 GHz, 6.24 GHz, and 7.5 GHz. The graph is plotted for performance comparison of S_{11} concerning frequency which is shown in Figure 10(b). The measured and simulated isolation parameter S_{12} is also added with S_{11} in Figure 10(b) for a better comparison. The measured and simulated radiation pattern graphs are plotted in Figure 12, corresponding to the desired resonance frequencies. After comparison, a slight deviation is observed in measured and simulated performances, as observed from Figures 10(b) and 12. This deviation is moderate, occurring due to the fabrication error while shorting pins are designed at feed locations.

The co-polar radiation patterns in E-plane and H-plane are measured using a measuring tool at the receiver end with AUT at desired resonance frequencies. The measured and simulated radiation patterns are both shown in Figure 12 for comparison.

Our proposed MPA performance is compared with the literature works available in the same area as listed in Table 5. In [19], an antenna is designed to operate in five modes using switches enabled with four PIN diodes. Each mode resonates either at the single band or multiple bands. This antenna is suitable for 5G handheld devices or IoT-enabled services. While our proposed antenna is simple in design, and it resonates at three bands in which one band is suggested for 5G in sub 6 GHz, while two others belong to backhauling bands above 6 GHz that make it suitable for base station antenna. In another research [20], a dual branch multi-band compact slotted antenna is presented, suitable for digital broadcasting, wireless, and sub 6 GHz for 5G applications. All these bands belong to different application

Table 5. Comparison of design and performance parameters of proposed work with available literature designs.

Ref.	Type of Antenna and Feed	The substrate used, Height of Substrate	No. of Resonance bands and f_O	Dimension of the Antenna	Maximum Gain/Div. Gain Achieved, Max.	Bandwidth Achieved	Techniques Used	Area of Application
Proposed Antenna	**Dual Feed Rectangular MPA**	**Roggers R03003, $\varepsilon_r = 3$, $h = 0.25$ mm**	**3, and f_C are 3.48, 6.24, 7.5 GHz**	**47.55× 51.88× 0.24 mm^3**	**9.8 dB**	**150, 310, 330 MHz**	**Orthogonal dual feed**	**5G, Mobile backhauling**
[19], 2021	Multimode resonance Antenna, Resonates maximum at three band in one mode	FR-4 substrate $\varepsilon_r = 4.3$, $h = 1.6$ mm	Mode 1: 5 GHz Mode 2: 3.5 GHz Mode 3: 2.6, 6.5 GHz Mode 4: 2.1, 5.6 GHz Mode 5: 1.8, 4.8, 6.4 GHz	40× 32× 1.6 mm^3	Mode 1: 1.25 dBi Mode 2: 2.17 dBi Mode 3: 1.76, 1.9 dBi Mode 4: 1.4, 2.15 dBi Mode 5: 1.2, 2.37, 3.6 dBi	Mode 1: 1400 MHz Mode 2: 1370 MHz Mode 3: 500, 670 MHz Mode 4: 300, 450 MHz Mode 5: 190, 580, 450 MHz	Switching Technique using 4 Pin Diode	5G Handheld Devices, IoT applications
[20], 2020	Multiband inverted E and U shaped compact antenna for Digital broadcasting, wireless, and sub 6 GHz 5G applications	FR-4 substrate $\varepsilon_r = 4.3$, $h = 1.6$ mm	0.77, 1.43, 2.13, 3.48, 3.84, 5.17, and 6 GHz	30× 30× 1.6 mm^3	1.1, 1.3, 1.1, 1.6, 1.7, 1.8, and 2.2 dBi	40, 40, 40, 70, 70, 60, 410 MHz	Inverted E and U shaped slots together	Digital Broadcasting, Medical telemetry, WLAN, WiMAX, Sub 6 GHz 5G, and Fixed Satellite Communication
[21], 2019	Quad-Band Dual-Arm Spiral Patch Antenna	FR-4 substrate $\varepsilon_r = 4.3$, $h = 1.6$ mm	915 MHz, 2.45 GHz, 3.5 GHz, 5.8 GHz	28× 28× 1.6 mm^3	−11.33, 1.17, 1.45, 1.96 dB	57, 116, 73, 206 MHz	CPW-fed technique with three slots and four L-shaped and two U- and F-shaped branches	RFID, WLAN and WiMAX Applications
[22], 2018	single element multiple feed antenna	FR-4 Epoxy, $\varepsilon_r = 4.4$, $h = 1.6$ mm	2, and f_C are 3.72 GHz, 9.40 GHz	24.5× 24.5× 1.6 mm^3	10 dB (Div. Gain), > -20 dB	5.680 GHz	T shape Dual Microstrip feed	WLAN, C-band applications
[23], 2018	Dual-feed CSRR-loaded switchable multiband using the square patch and square-ring patch	Rogers RT/duroid, 5880), $\varepsilon_r = 2.2$, $h = 3$ mm	7, 1.93, 3.73, 4.35, 5.9, 6.35, 7.25, and 8.75 GHz	100× 100× 3 mm^3	9.9 dBi, > -16 dB	50, 50, 500, 200, 300, 600 MHz	Dual-feed with co-axial feeding, and short-ended microstrip feeding	intelligent transportation system
[24], 2016	A switchable co-planar linearly polarized multi-band MPA	Rogers RT/duroid 5880), $\varepsilon_r = 2.2$, $h = 1.57$ mm	7, Tunable 4.73, 5.93, 7.16, 7.43, 11.08, 13.3, 16.85 GHz	96× 96× 1.57 mm^3	8 dB, > -11 dB	150, 600, 450, 650, 1350, 2650 MHz	Switching technique, (Two slotted square patches with the different dimensions and shapes)	ITS, WLAN, WiMAX, Direct broadcast satellite

groups, while our proposed antenna can be used for 5G base station service simultaneously resonating at 5G communication bands and backhauling bands. In [21], a multi-band antenna is designed for applications such as RFID, WLAN, and WiMAX from different service groups compared to our proposed design for multi-band, suitable for 5G base station. In research [22], a single element with a dual-feed having rectangular slot cutting is presented, and the antenna resonates at two bands. These bands do not belong to the same service group, whereas the proposed antenna used in this research resonates at three bands that belong to the same application group. In [23], the designed antenna has two patches that are excited by two microstrip feeds. This antenna is loaded with two PIN diodes. Switching the diodes results in different resonance frequency bands. The antenna resonates at seven different bands where bands' applications are not precise and justified for a single application. In our case, it is justified and according to suggestions of ITU-R. The antenna structure is complicated compared to our proposed antenna. In [24], two slotted square patches having different dimensions and slot cuttings are cascaded. Switching between patches is possible with the help of a PIN diode. The antenna resonates at seven

bands that do not belong to the dedicated applications. The antenna structure dimension is almost double compared to our proposed antenna designed for a reliable application.

Our proposed design seems simple after all these literary works are compared, but all resonating bands belong to the same application area. Apart from these, our proposed antenna design is better than other designs available in the literature [19–24]. Out of its three resonance bands, the band resonating at 3.48 GHz generates a fully circularly polarized wave. It means that the user's orientation does not affect the signal quality received by the user's device. The other two bands are moderately circularly polarized, although circular polarization is not essential due to base station antennas' fixed orientation. Our proposed design is verified in two simulation environments, HFSS and MATLAB. The proposed antenna is further tested in a real-time application environment in MATLAB to create 5G cellular sites, as discussed in the next real-time application section.

7. REAL-TIME APPLICATION

7.1. Dual-Feed MPA Design in MATLAB

As mentioned in Table 2, these optimized parameters are utilized further for the antenna design in MATLAB software. After the simulation, parameters such as resonance frequency and the value of reflection coefficient in every three bands are noted and compared in Table 6. However, parameters obtained after simulation in MATLAB, such as resonance frequency and the value of the reflection coefficient for all three bands are a little deviated from HFSS, as shown in Table 6. The reflection-coefficient versus frequency graph of HFSS and MATLAB merged in a single figure for comparison concludes the same. The dual-feed antenna structure modeled in MATLAB is also incorporated in the same Figure 13.

Table 6. Comparison of resonance frequency and S_{11} in HFSS and MATLAB for different bands.

Band (GHz)	HFSS		MATLAB	
	Resonance frequency (GHz)	S_{11} (dB)	Resonance frequency (GHz)	S_{11} (dB)
3.3 GHz–3.7 GHz	3.48	−27.77	3.624	−14.95
5.925 GHz–6.425 GHz	6.24	−28.8	6.07	−22.82
7.11 GHz–7.9 GHz	7.5	−33.98	7.368	−20.55

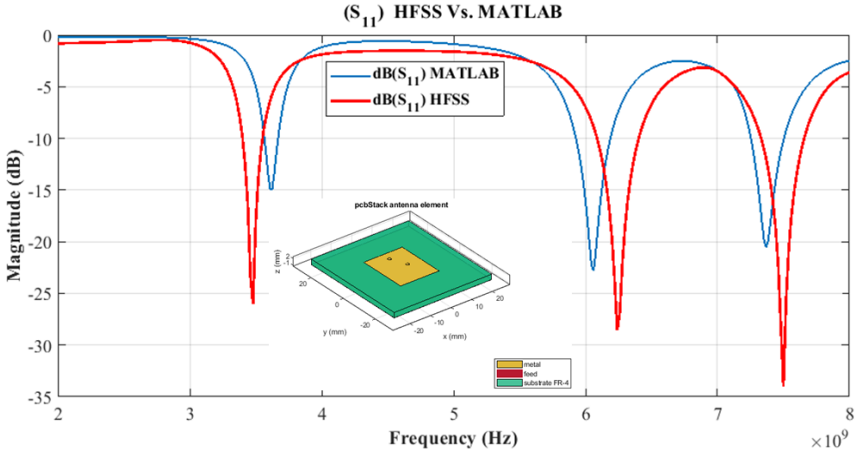

Figure 13. Reflection-coefficient S_{11} vs. frequency of HFSS and antenna modeled in MATLAB.

7.2. Cellular Sites for 5G

A real-time application environment for 5G cellular, is visualized in MATLAB. 5G cellular networking is in realization, with 19 cellular sites and each cellular site with three cells, i.e., a total of 57 cells. As discussed above, the proposed MPA antenna designed in MATLAB is placed in each cell for the user's communication band, i.e., the frequency range, 3.4737 GHz to 3.5489 GHz, at center frequency 3.48 GHz. So a total of 57 antennas are required for the 5G cellular network as mentioned above. The cellular network is developed with 19 cellular sites with an inter-site distance being 200 meters, as shown in Figure 14.

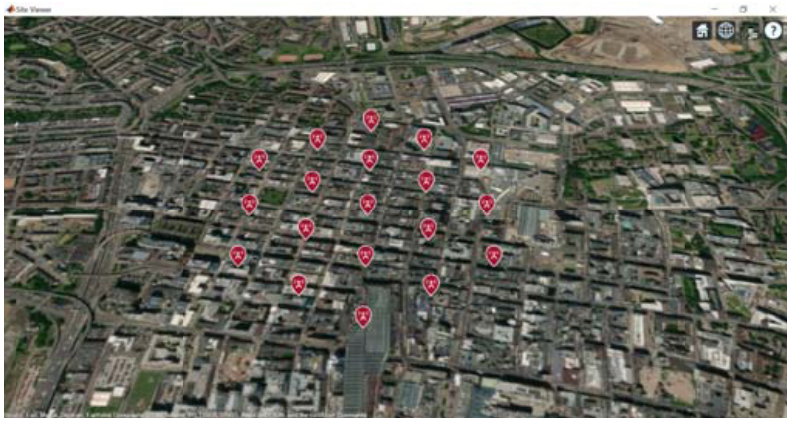

Figure 14. 5G cellular network with 19 cellular sites with the inter-site distance of 200 meter.

7.3. Proposed MPA Used for BTS to User Communication

The antenna used in the lab environment is along the XY plane, and its pattern is in the Z plane perpendicular to the XY plane, as shown in Figure 15(a). When being used on BTS, the same antenna is placed in the YZ plane, and its radiation pattern is along the X-axis, as shown in Figure 15(b). The antenna is placed at some height to find a better LOS with users for successful communication. Intended users or any object lies on the XY plane, although its height is towards the direction of antenna height, i.e., in the Z-axis. So radiated signal will be in the X direction, i.e., user's direction and out of reach for

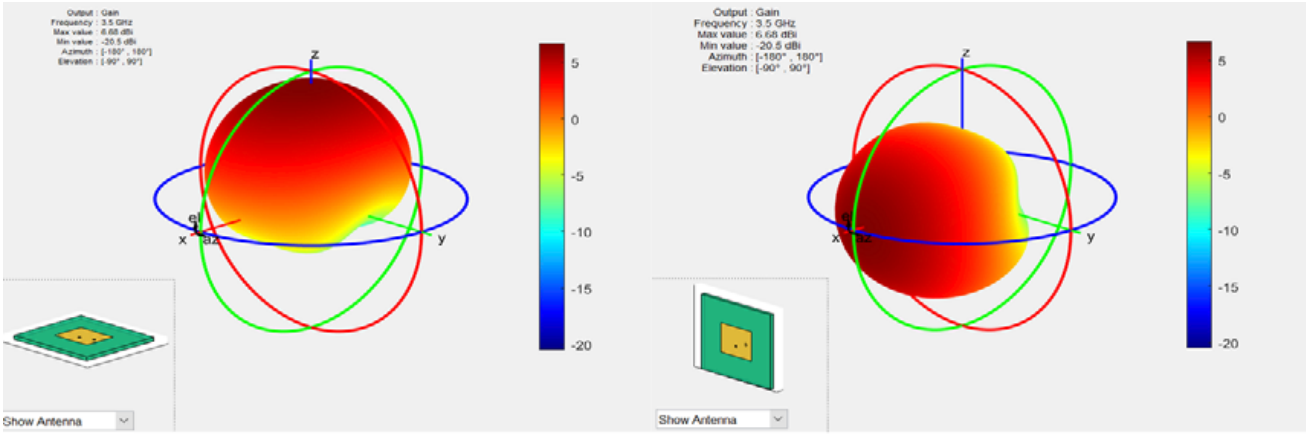

Figure 15. Antenna and its radiation pattern (a) when not used on cell sites, (b) when used on cell sites (rotated 90 degrees).

intended users due to height mismatch. The antenna is tilted towards users' geographical location at 15 degrees to cover the height mismatch and make this radiated signal useful. Installation of individual antenna for a particular cell total of 57 antennae is needed, with each having less directivity and more broadside coverage while less radial coverage results in more considerable interference. To minimize this interference array of the antenna is useful due to enhanced directivity and less broadside coverage. These concepts, as mentioned above, are considered while a real-time scenario is created for 5G cellular.

An 8×8 array of the same antenna element with spacing $\lambda/2$ is used for a single cell to enhance the directivity and minimize the interference. Figure 16(a) shows the directivity pattern of 8×8. Figure 16 (b) shows the SINR map of the whole cellular network if there is no tilt of the array's antenna element. The same 8×8 antenna array having the 15-degree inclination on BTS shows improved SINR, as shown in Figure 16(c).

(a) (b) (c)

Figure 16. (a) Directivity, (b) SINR map without tilt, (c) SINR map with a tilt of 8×8 array antenna.

7.4. Proposed MPA Used for BTS to BTS Communication

The radiation patterns of a single element in HFSS at 6.24 GHz and 7.5 GHz are not broadsided, as shown in Figure 6. The same limitation is also considered for the single antenna element designed in MATLAB. However, the beamforming of the antenna array is realized in MATLAB to broaden the radiation pattern. A highly directive and pointed main beam is generated using beamforming and focused towards the desired direction for BTS to BTS backhauling communication for 5G cellular. The

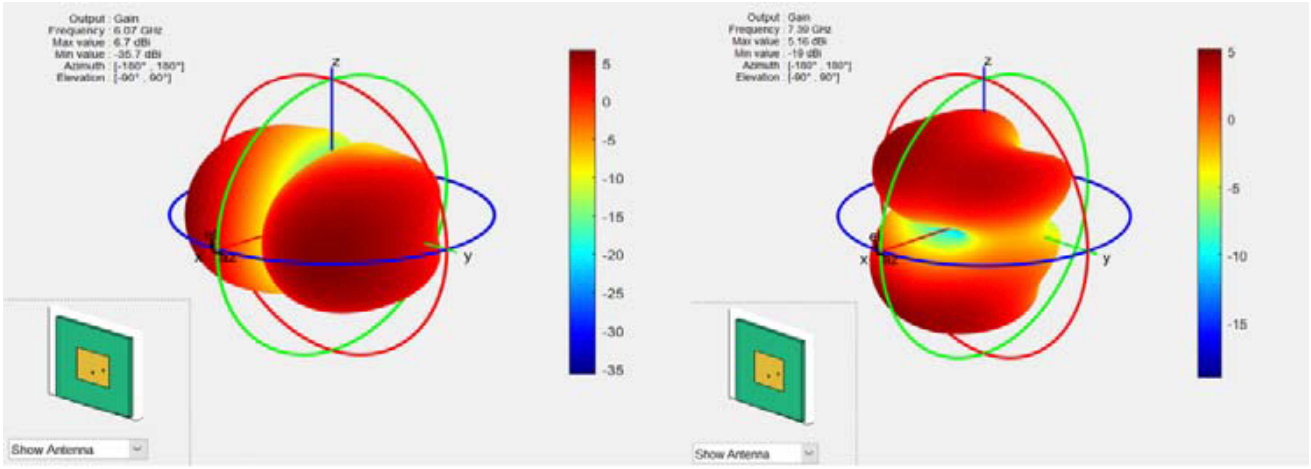

(a) (b)

Figure 17. Antenna and its radiation pattern (a) at 6.07 GHz, (b) at 7.39 GHz.

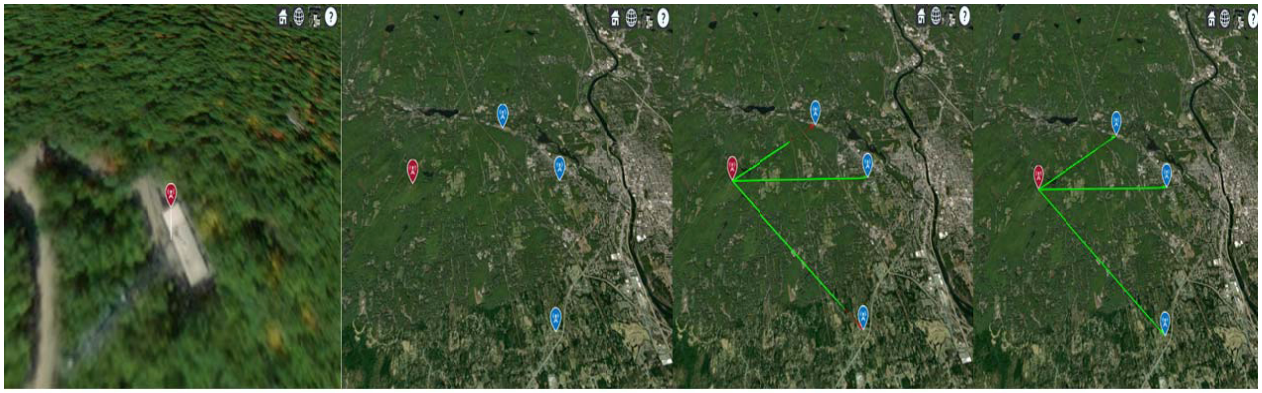

(a) (b) (c) (d)

Figure 18. (a) Transmitter BTS. (b) Transmitter BTS with three-receiver BTSs. (c) LOS between transmitter BTS and receiver BTS not achieved due to BTS height. (d) LOS achieved between transmitter BTS and receiver BTS with increased BTS height.

antenna designed in MATLAB resonates on two more bands proposed for mobile backhauling used for the base station to base station communication. These bands are 5.9398 GHz to 6.2105 GHz, 7.2782 GHz to 7.5489 GHz which resonate at 6.07 GHz, and 7.39 GHz. Real-time realization of antenna designed in MATLAB is explained below. Figures 17(a) and 17(b) show a single antenna's radiation pattern at frequencies 6.07 GHz and 7.39 GHz. Figures of real-time implementation are almost the same for these two bands. Due to this, the implementation figure of only a single band, i.e., 5.9398 GHz to 6.2105 GHz having a center frequency at 6.07 GHz, is presented. However, their data are presented separately for both situations. Figure 18(a) shows that a transmitter site is created only for the communication between BTS and BTS, i.e., backhauling purpose at South Uncanoonuc, whose latitude and longitude are 42.983723, −71.587173, respectively. The transmitter site created is equipped with a multi-band antenna developed in MATLAB that resonates at 6.07 GHz. Figure 18(b) shows three other BTSs sites designed simultaneously to carry forward the received signal from the previous backhauling BTS. These locations are considered from abroad countries intentionally to realize the worst situation for 5G cellular due to heavy and heightened infrastructure. The site locations of these BTSs is Bedford Town Center having latitude, 42.946193, longitude, −71.516234, St. Anselm College having latitude, 42.987386, longitude, −71.507475, and Goffstown Police Dept having latitude, 43.009335, longitude, −71.539083. Initially, all these site locations' heights are 6 meters, 6 meters, and 15 meters respectively and checked for a line of sight among these four BTSs. Figure 18(c) shows that a check for line of sight in between these BTSs remains unsuccessful. In Figure 18(d) BTSs heights are increased stepwise, and it is found that they achieve a line of sight at 70 meters. The achieved Directivity and coverage enhancement

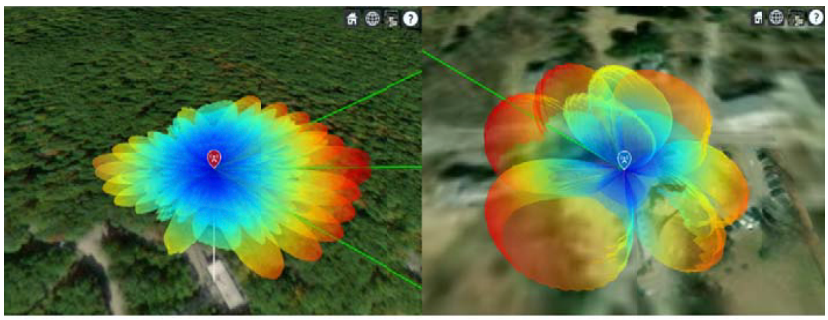

(a) (b)

Figure 19. Beamforming pattern of the antenna array (a) at transmitter BTS, (b) at receiver BTS.

of the transmitter BTS using the antenna array with array size 12×8 of the designed antenna element with its beamforming pattern is shown in Figure 19(a). While receiver BTS has an antenna array with an array size of 3×3 of the same designed antenna element, its beamforming pattern is shown in Figure 19(b). These receiver BTSs' direction towards transmitter BTS and the beamforming concept are utilized for communication between them. The beamforming of the transmitter BTS antenna array towards each receiver BTS antenna array individually is shown in Figure 20. From Figure 20, it can be observed that the antenna array structure having the proposed antenna as its element has a highly directive radiation pattern towards the desired direction. This radiation property makes the proposed antenna and array suitable for 5G mobile backhauling applications. The beamforming of the transmitter BTS antenna array towards each receiver BTS antenna array simultaneously is shown in Figure 21.

All these scenario signal strengths are fetched from simulation software, noted, and compared in Table 7. Apart from these scenarios, some additional noise environment is created, and losses due to foliage, heavy rain, and signal strengths are fetched from software tools, recorded, and compared for all these scenarios.

Table 7. Performance parameters measured at different cellular sites in MATLAB.

S.No.	Different Environment	Power Measured in dBm From Transmitter BTS		
		To Bedford Town Center	To St. Anselm College	To Goffstown Police Dept
For Resonance band 5.9398 GHz to 6.2105 GHz at center frequency 6.07 GHz				
1.	**In the case of individual communication between transmitter and receiver in dBm**	−67.8246	−68.9051	−64.5191
2.	**In case of simultaneous transmission in dBm**	−71.0645	−81.4692	−67.7286
3.	**Addition of Path Loss due to foliage (−14.7321 dBm) in dBm**	−85.7966	−96.2014	−82.4608
4.	**After the addition of heavy rain in between 4 mm to 16 mm per hour in dBm**	−86.144	−96.5243	−82.7135
For Resonance band 7.2782 GHz to 7.5489 GHz at center frequency 7.39 GHz				
1.	**In the case of individual communication between transmitter and receiver in dBm**	−68.6528	−71.023	−65.8439
2.	**In case of simultaneous transmission in dBm**	−72.1912	−78.5722	−69.7134
3.	**Addition of Path Loss due to foliage (−15.5788 dB)**	−87.77	−94.151	−85.2922
4.	**After the addition of heavy rain in between 4 mm to 16 mm per hour**	−88.5901	−94.9135	−85.8891

(a) (b) (c)

Figure 20. Beamforming towards (a) first receiver BTS, (b) second receiver BTS, (c) third receiver BTS.

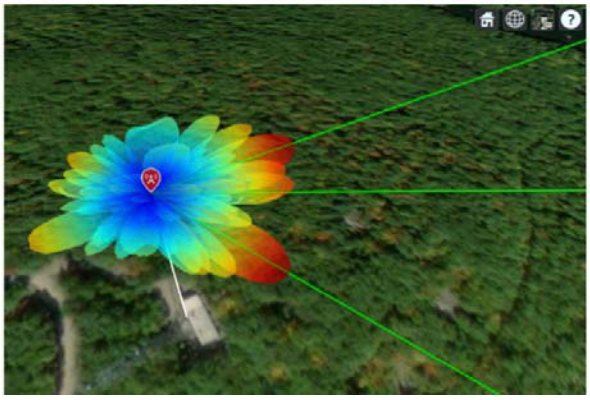

Figure 21. Beamforming towards each receiver simultaneously.

8. CONCLUSION

A dual-feed multi-band MPA was modeled and simulated initially in HFSS. Feed locations and other parameters were optimized successfully using parametric optimization in HFSS. Sound isolation was achieved due to optimized feed locations between two ports, and the fabrication of a prototype antenna became possible. The proposed MPA resonates at multiple bands for the desired applications with adequate 10 dB return loss bandwidth, fully circularly polarized at 3.48 GHz while moderately polarized at two other bands. Fabrication of the MPA became possible with optimized parameters; results were measured in an anechoic chamber and compared with the HFSS simulation result. A comparison was performed between measured S_{11} and simulated S_{11} of HFSS, and they were closely following. The measured and simulated co-planar radiation patterns in both E-plane and H-plane were also matched. The proposed MPA was modeled in MATLAB, and its reflection coefficient S_{11} was measured. Measured S_{11} is slightly deviated from the S_{11} of HFSS simulation. Finally, this proposed antenna was modeled in MATLAB for users' communication at 5G BTSs and backhauling inter BTSs communication and tested in MATLAB simulation scenarios for real-time applications.

In the first situation, 19 cellular 5G sites were built, each with three cells. Cellular sites have used this proposed MPA and its arrays. SINR pattern for these cellular sites was pictured initially and further investigated for improved SINR. Better SINR was achieved with antenna tilting. In another situation of inter-BTS communication, an example of backhauling was created for the above-mentioned backhauling bands. Here, one cellular transmitter site was communicated with three cellular receiver sites using these backhauling bands. Two array structures of 12×8 and 3×3 were created using the proposed multi-band

antenna for the transmitter and receiver cellular sites, respectively. Intercommunications between these sites were visualized using beamforming of these arrays. Finally, the design and implementation in real-time simulation environments of the MPA were successful, and the measured signal strength was in the standard prescribed range.

REFERENCES

1. Wu, Z., V. Park, and J. Li, "Enabling device to device broadcast for LTE cellular networks," *IEEE Journal on Selected Areas in Communications*, Vol. 34, No. 1, 58–70, 2016.
2. Qiao, J., X. Shen, J. W. Mark, Q. Shen, Y. He, and L. Lei, "Enabling device-to-device communications in millimeter-wave 5G cellular networks," *IEEE Communications Magazine*, Vol. 53, No. 1, 209–215, 2015.
3. Feng, D., L. Lu, Y. Yuan-Wu, G. Y. Li, S. Li, and G. Feng, "Device-to-device communications in cellular networks," *IEEE Communications Magazine*, Vol. 52, No. 4, 49–55, 2014.
4. Rysavy Research/5G Americas, "LTE to 5G," August 2018. [Online]. Available: http://www.5gamericas.org/files/4915/3479/4684/2018_5G_Americas_Rysavy_LTE_to_5G-The_Global_Impact_of_Wireless_Innovation_final.pdf.
5. Doppler, K., M. Rinne, C. Wijting, C. B. Ribeiro, and K. Hugl, "Device-to-device communication as an underlay to LTE-advanced networks," *IEEE Communications Magazine*, Vol. 47, No. 12, 42–49, 2009.
6. Rubio-Drosdov, E., D. Díaz-Sánchez, F. Almenárez, P. Arias-Cabarcos, and A. Marín, "Seamless human-device interaction in the internet of things," *IEEE Transactions on Consumer Electronics*, Vol. 63, No. 4, 490–498, 2017.
7. Bello, O. and S. Zeadally, "Intelligent device-to-device communication in the internet of things," *IEEE Systems Journal*, Vol. 10, No. 3, 1172–1182, 2016.
8. Voicendata Bureau, "Voice & data," August 14, 2018. [Online]. Available: https://www.voicendata.com/5g-will-gateway-new-technologies-services-applications/.
9. Kassem, M. M. and M. K. Marina, "Future wireless spectrum below 6 GHz: A UK perspective," *2015 IEEE International Symposium on Dynamic Spectrum Access Networks (DySPAN)*, Stockholm, Sweden, 2015.
10. ITU R, "Agenda and Relevant Resolutions WRC-19," August 15, 2017. [Online]. Available: http://handle.itu.int/11.1002/pub/80f52158-en.
11. Kavanagh, S., "5G.CO.UK," 2019. [Online]. Available: https://5g.co.uk/guides/4g-versus-5g-what-will-the-next-generation-bring/.
12. ITU, "Fixed service use and future trends," November 2017. [Online]. Available: https://www.itu.int/pub/R-REP-F.2323.
13. GSM Association, "GSMA," September 2018. [Online]. Available: https://www.gsma.com spectrum/wp-content/uploads/2019/04/Mobile-Backhaul-Options.pdf.
14. Anzaldo, D., "Backhaul alternatives for 4G/5G," 2014. [Online]. Available: https://pdfserv.maximintegrated.com/en/an/AN6544.pdf.
15. Pozar, M. D., *Microwave Engineering*, 4th Edition, John Wiley & Sons, Inc., Amherst, 2012.
16. Balanis, C. A., *Antenna Theory Analysis and Design*, A John Wiley and Sons, Inc., Hoboken, New Jersey, 2005.
17. Kumar, G. and K. P. Ray, *Broadband Microstrip Antennas*, Artech House, London, 2003.
18. Garg, R., P. Bhartia, I. Bahl, and A. Ittipiboon, *Microstrip Antenna Design Handbook*, Artech House, London, 2001.
19. Dildar, H., F. Althobiani, I. Ahmad, W. Khan, S. Ullah, N. Mufti, S. Ullah, F. Muhammad, M. Irfan, and A. Glowacz, "Design and experimental analysis of multiband frequency reconfigurable antenna for 5G and sub-6 GHz wireless communication," *Micromachines*, Vol. 12, No. 1, 32, 2021.

20. Desai, A., R. Patel, T. Upadhyaya, H. Kaushal, and V. Dhasarathan, "Multi-band inverted E and U shaped compact antenna for Digital broadcasting, wireless, and sub 6 GHz 5G applications," *International Journal of Electronics and Communications (AEÜ)*, Vol. 123, 153296, August 2020.
21. Jabar, A. A. S. A. and D. K. Naji, "Design of miniaturized quad-band dual-arm spiral patch antenna for RFID, WLAN and WiMAX applications," *Progress In Electromagnetics Research C*, Vol. 91, 97–113, 2019.
22. Roobini, A. and B. Sreeja, "Design and analysis of single element multiple feed antenna for wide band dual polarisation applications," *International Journal of Pure and Applied Mathematics*, Vol. 118, 1–12, 2018.
23. Upadhyay, G., N. Kishore, S. Raj, S. Tripathi, and V. S. Tripathi, "Dual-feed CSRR-loaded switchable multi-band microstrip patch antenna for ITS applications," *IET Microwaves, Antennas & Propagation*, Vol. 12, 2135–2140, 2018.
24. Upadhyay, G. and V. S. Tripathi, "Pin-diode based switchable multi-band dual feed microstrip patch antenna," *Microwave and Optical Technology Letters*, Vol. 59, No. 6, 1454–1460, 2016.
25. "IEEE standard definitions of terms for antennas," IEEE Std 145-1993, 1–32, July 18, 1993, doi: 10.1109/IEEESTD.1993.119664.